Chemical Technology & Biotechnology, 2024, pp. 115-120

Aggregation analysis of laser generated silver-109 nanoparticles

Artur Kołodziej*

Rzeszów University of Technology, Faculty of Chemistry, 6 Powstańców Warszawy Ave., 35-959 Rzeszów, Poland

ABSTRACT

This study investigates the aggregation behavior of stabilizer-free silver-109 nanoparticles synthesized *via* laser ablation synthesis in solution (LASiS) using a pulsed fiber laser equipped with a 2D galvoscanner. High-resolution scanning electron microscopy (HR SEM) imaging and laser desorption/ionization mass spectrometry (LDI MS) were employed to analyze changes in nanoparticle morphology and silver-109 clusters signal intensity, providing insights into their stability and performance.

Keywords: silver nanoparticles, aggregation, SEM, LDI MS, mass spectrometry

1. Introduction

Silver nanoparticles (AgNPs) possess unique physical properties, including a high surface-to-volume ratio, excellent electrical conductivity, and localized surface plasmon resonance (LSPR) [1], enabling strong light absorption and scattering. These properties make them valuable in applications such as biosensing [2], imaging [3], and advanced electronics [4]. AgNPs are utilized in wound dressings, coatings for medical devices, and drug delivery systems due to their antimicrobial and antiviral properties [5], which help prevent infections and promote healing. Their optical and thermal stability further enhance their functionality in diagnostic tools and treatments [6].

AgNPs play a critical role in enhancing laser mass spectrometry techniques, particularly in surface-assisted laser desorption/ionization mass spectrometry (SALDI-MS). Their unique optical properties, including LSPR, amplify the laser energy absorption, enabling efficient desorption and ionization of analytes. This enhances sensitivity and detection limits, making AgNPs ideal for analyzing low-concentration biomolecules, small organic compounds, and environmental pollutants [7, 8]. Additionally, the high surface area of AgNPs provides abundant interaction sites for target molecules, further improving signal intensity. Their use in SALDI-MS contributes to advancements in proteomics, metabolomics, and forensic analysis by enabling precise and rapid molecular characterization [9, 10].

The size of silver nanoparticles significantly influences their physical, chemical, and biological properties [11]. Due to their higher surface-area-to-volume ratio, smaller nanoparticles exhibit enhanced reactivity and stronger antimicrobial effects [12, 13]. They also demonstrate more pronounced optical properties, with a shift in LSPR peaks depending on particle size, which is critical for applications like sensing and imaging. However, smaller AgNPs are more prone to aggregation, as their high surface energy drives instability. Aggregation alters their size distribution, diminishes their unique properties, and reduces their effectiveness in applications [14]. Stabilizers or surface modifications are often employed to mitigate aggregation and preserve their functional characteristics.

The publication presents the results of the study of the aggregation of stabilizer-free silver-109 nanoparticles synthesized by the laser absorption synthesis in solution (LASiS) method using a pulsed fiber laser equipped with a 2D galvoscanner. The solvent for synthesis was acetonitrile, which was chosen due to earlier studies on the

* Corresponding author at: Rzeszów University of Technology, Faculty of Chemistry, 6 Powstańców Warszawy Ave. , 35-959 Rzeszów, Poland; *E-mail*: a.kolodziej@prz.edu.pl

https://doi.org/10.7862/rc.2024.8

Received 9 December 2024; Received in revised form 16 December 2024; Accepted 16 December 2024; Available online 18 December 2024

e-ISSN 2720-6793. Published by Publishing House of Rzeszów University of Technology.

influence of the solvent on the quality of MS spectra. The paper presents the results of high resolution scanning electron microscopy (HR SEM) imaging, and an analysis of the change in the intensity of the silver-109 cluster signals using LDI MS was also performed.

2. Experimental

2.1. Materials

A silver-109 isotope of 99.7% isotopic purity was bought from Trace Sciences International (USA). Stainless steel targets were machined from H17 stainless steel polished to the mirror finish. The silicon wafer was purchased from a local manufacturer. Before the experiment, steel targets were cleaned by dipping them in boiling solvents: toluene, chloroform, acetonitrile, and deionized water. Toluene and chloroform were analytically pure, acetonitrile was of HPLC grade, and water 18 MΩcm^2 was produced locally.

2.2. Methods

2.2.1 Synthesis of ^{109}Ag nanoparticles

Silver-109 foil was put into the beaker, and then acetonitrile was added. Laser ablation was then performed using a pulsed fiber laser (Raycus, Wuhan, China) with a wavelength of 1064 nm. Nitrogen was used as an inert gas. A detailed protocol for the synthesis of ^{109}AgNPs by using laser ablation with the pulsed fiber laser is available in a previous publication [15].

2.2.2 ^{109}Ag nanoparticles aggregation study

After synthesis, the nanoparticle suspension was applied using a pipette onto the surface of steel and silicon plates at designated time intervals. These time intervals were: immediately after synthesis (0 h), 1 h, 12 h, 24 h, and 168 h (7 days) after synthesis. The nanoparticles in suspension were stored in an Eppendorf at room temperature, from which they were stirred and applied onto the plate's surface after the previously mentioned time. After the last application of the nanoparticle suspension, both plates were examined using HR SEM. Stainless steel plate was also used in LDI MS analysis. For each given time, a single spot of the nanoparticle suspension was applied to both plates, which were then subjected to the described analyses"

2.2.3 High-resolution scanning electron microscopy (HR SEM)

The targets modified with ^{109}AgNPs generated by the pulsed fiber laser equipped with a 2D galvoscanner (PFL 2D GS) method were inserted into the Helios Nanolab 650 electron microscope. Voltage was set at 10 and 30 kV, current was 0.2 nA. Images were made in nonimmersive mode.

2.2.4 LDI MS experiment

LDI-ToF-MS experiments were performed in reflectron mode using a Bruker Autoflex Speed time-of-flight mass spectrometer equipped with a SmartBeam II laser (355 nm). Laser impulse energy was approximately 90-140 μJ, and the laser repetition rate was 1000 Hz. The total number of laser shots was 4000 for each spot divided into packs of 1000 shots per measurement point. At each point, 1000 laser shots were made with default random walk applied (random points with 50 laser shots). The measurement range was *m/z* 80–1500. Suppression was turned on typically for ions of *m/z* lower than 80. Reflector voltages were 21 kV (the first) and 9.55 kV (the second). The data were calibrated and analyzed with FlexAnalysis (version 3.3) using a centroid calibration model. Mass calibration (enhanced cubic calibration based on 7 calibration points) was performed using internal standards (silver-109 ions and clusters from $^{109}Ag^+$ to $^{109}Ag_7^+$)

3. Results and discussion

Using the laser generation nanomaterial (LGN) method with a pulsed fiber laser equipped with a 2D galvoscanner, chemically pure silver-109 nanoparticles suspended in acetonitrile were obtained. The size of the ^{109}Ag nanoparticles was about 50-60 nm, which is consistent with the results presented in the publication describing the synthesis process of these nanoparticles [15]. Detailed information on the properties and methods of characterization of the obtained nanoparticles was also described in this publication.

3.1 High-resolution SEM results

The plates covered with nanoparticles were delivered to the Centre for Micro and Nanotechnology at the University of Rzeszów. Images were taken for the tested aggregation times on steel and silicon plates. The collected HR SEM imaging results are presented in Figures 1 and 2.

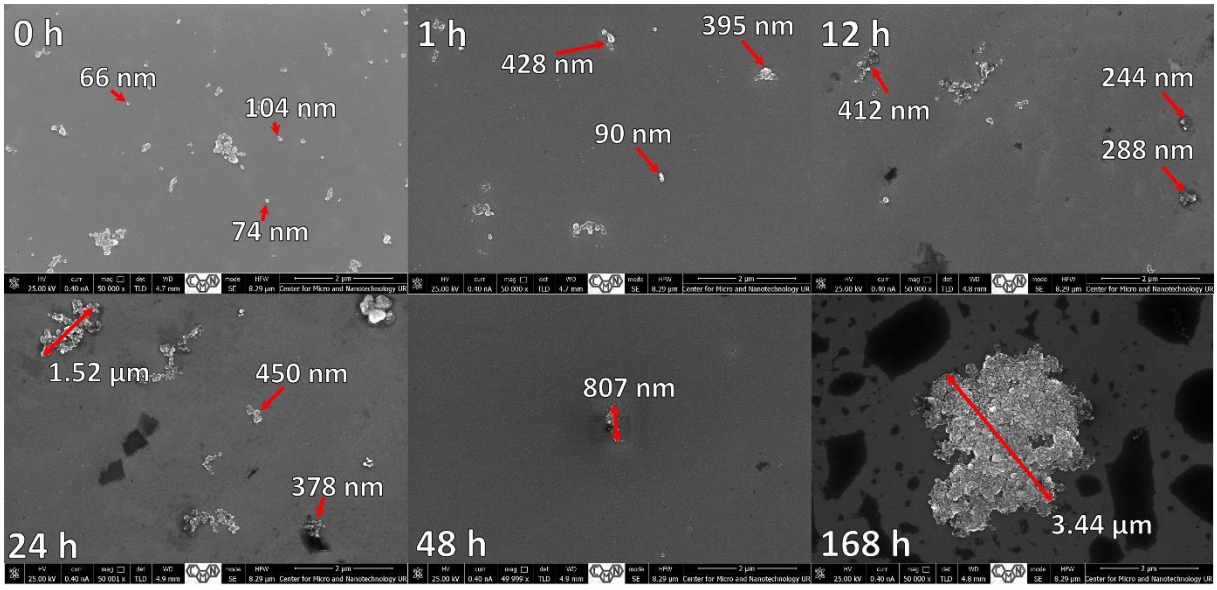

Fig. 1. HR SEM images of silver-109 nanoparticles and aggregates on a silicon wafer.

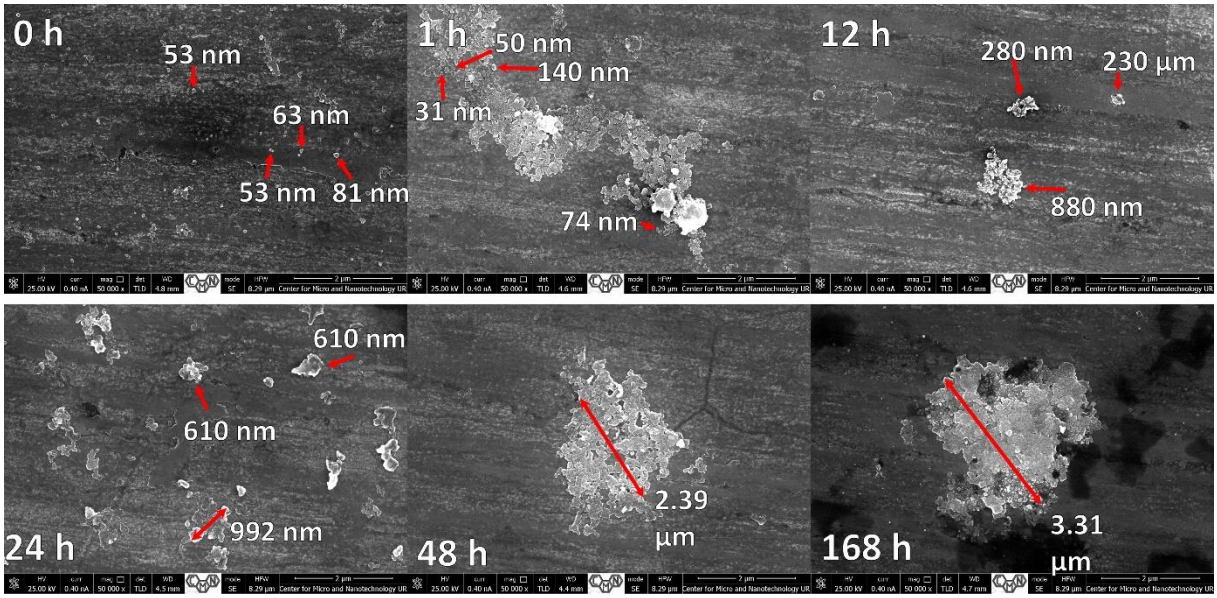

Fig. 2. HR SEM images of silver-109 nanoparticles and aggregates on a stainless steel plate.

In both images taken on spots applied directly after the synthesis of ^{109}AgNPs (Fig. 1 0 h and Fig. 2 0 h), we can see the presence of single nanoparticles with a ca. 50-70 nm diameter. The next spot was applied 1 hour after the synthesis of nanoparticles. The image of the silicon wafer (Fig. 1. 1 h) shows aggregates of nanoparticles with a diameter of about 400 nm, however, the image still shows single nanoparticles with a diameter of less than 100 nm. On the steel plate (Fig. 2. 1 h), a large nanoparticle complex can be seen, making it possible to indicate single ^{109}AgNPs adjacent to this structure. Fig. 1. 12 h and Fig. 2. 12 h show the nanoparticle aggregates obtained after the suspension was applied 12 h after synthesis. In both cases, we see aggregates with a diameter of 250-400 nm. On the silicon wafer, there are still single larger nanoparticles, but on the steel plate, there are only ^{109}Ag aggregates. In the last three images of the silicon wafer, we see only nanoparticle aggregates that increase their diameter. The diameter of the aggregates 24 h after synthesis varies between 0.4-1.5 µm. Finally, 7 days after the synthesis of ^{109}AgNPs, a single huge aggregate with a diameter of about 3.44 µm is visible. On the steel plate, the size of the aggregates 24 h after synthesis is about 600 nm, in the microscopic image many structures of this size are visible. The last two HR SEM images (Fig. 2. 24 h and 48 h) show single aggregate structures composed of groups of smaller aggregates with diameters of 2.39 µm and 3.31 µm, respectively.

3.2 LDI mass spectrometry analysis of stainless steel plate with aggregates

After the last measuring point was applied, the stainless steel plate covered with spots of the nanoparticle and aggregate suspension was placed in a MALDI-ToF mass spectrometer. The obtained mass spectra allowed for indicating the signal intensities for five ^{109}Ag clusters. Table 1 presents the exact *m/z* values calculated using the Chemcalc mass calculator for the tested ^{109}Ag ions. Based on these data, Fig. 3 was prepared.

Table 1. The *m/z* values for tested silver-109 ions and clusters.

^{109}Ag cluster	*m/z* value
$^{109}Ag^+$	108.9042
$^{109}Ag_2^+$	217.8090
$^{109}Ag_3^+$	326.7137
$^{109}Ag_4^+$	435.6185
$^{109}Ag_5^+$	544.5232

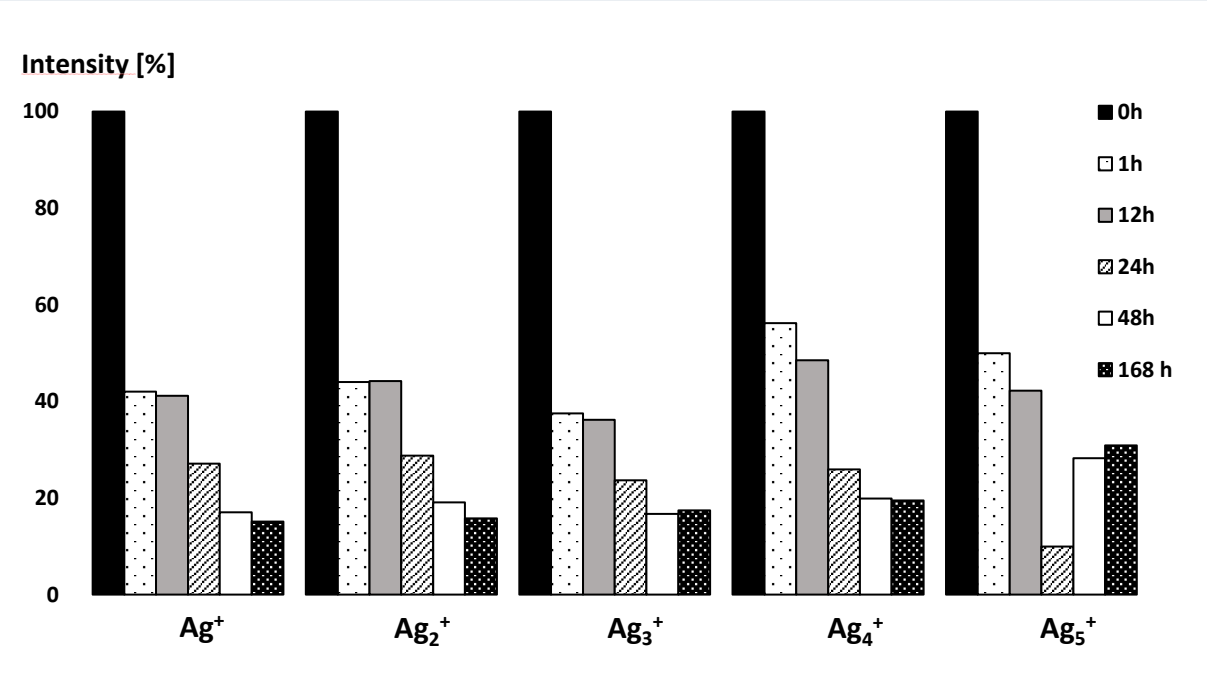

Fig. 3. Graph showing the changes in intensity values as a function of time for silver-109 clusters.

Fig. 3. presents the changes in the intensity values for the signals of silver-109 and its clusters. For each case, the intensity value measured for the samples applied immediately after synthesis (approx. 3-5 minutes from applying the sample on the plate until the end of the measurement in the MALDI-ToF instrument) is calculated as 100%. The intensity values after the time from synthesis are calculated as a percentage of the initial intensity value. In the case of Ag^+ and Ag_2^+, the signal intensity value decreases with time, which means that there are fewer of these ions on the spot. For the Ag_3^+ cluster, we see a decrease in intensity in the range of 1-48 h, while the relative signal intensity after 168 h is slightly higher than the signal after 48 h. In the case of the Ag_4^+ cluster, the intensity decreases with time. However, it is worth noting that the relative intensity of the signals 1 h and 12 h after synthesis is much higher than in the three previous cases approx. 60% of the initial intensity after 1 h for Ag_4^+ compared to approx. 40% for Ag^+ and ~55% for Ag_4^+ after 12 h *vs* 40% for Ag^+. In the case of the Ag_5^+ cluster the decrease in intensity value is also smaller than in the case of the Ag^+, Ag_2^+, and Ag_3^+ clusters. The relative intensity reaches a minimum of 24 h after synthesis for this cluster and is the lowest to the initial value for all presented cases, however, after 48 and 168 h the relative intensity increases about 2.5-3 times compared to the value 24 h after the synthesis of nanoparticles. These intensities are also higher than the values of all other clusters, which suggests that smaller clusters aggregated to larger clusters. The results presented in this section also confirm the occurrence of the aggregation process of silver-109 nanoparticles synthesized by the LASiS method.

The results presented in the publication are consistent with literature data indicating the tendency of silver nanoparticles to aggregate in an aqueous environment [16, 17]. However, in the presented studies, the aggregation

of nanoparticles is studied in water and not in acetonitrile as in the case of the presented results. The literature data also indicate an important effect of the ionic strength of the solution on the aggregation of nanoparticles. Prathna *et al*. [18] indicate that an increase in the concentration of sodium nitrate affects the change of the SPR peak, which causes the absorption maximum change and the broadening of the peak in the UV-Vis spectra. Smaller nanoparticles, typically *ca.* 10 nm, exhibit higher surface energy and enhanced plasmonic effects, promoting more efficient energy transfer during laser irradiation [11], which is a desirable phenomenon in the laser desorption/ionization process. Conversely, larger nanoparticles may provide better thermal stability but reduce desorption/ionization efficiency due to decreased surface-area-to-volume ratio and less localized plasmon resonance [19] reducing the efficiency of ion formation in LDI MS.

3.4. Conclusions

The publication presents the results of the study of the aggregation of silver-109 nanoparticles synthesized by the LASiS method using 2D GS PFL. A stabilizer-free suspension of nanoparticles in acetonitrile was obtained. HR SEM and LDI MS studies showed that over time the aggregation process of ^{109}AgNPs takes place following the theoretical assumptions given in the literature, affecting the size and physicochemical properties of the obtained nanoparticles. Studies using a MALDI-ToF mass spectrometer also confirm the occurrence of the nanoparticle aggregation process, which is visible as a decrease in the intensity values for $^{109}Ag^+$ - $^{109}Ag_4^+$ ions for the tested periods after synthesis and intensity increase for the $^{109}Ag_5^+$ cluster after 48 h and 168 h. Controlling the aggregation process of silver nanoparticles (AgNPs) is crucial for enhancing their practical applications across various fields. In biomedical applications, maintaining stable, non-aggregated AgNPs is essential for ensuring consistent antibacterial activity and drug delivery efficiency, as aggregation can reduce their bioavailability and surface reactivity. In sensing technologies, preventing aggregation helps preserve their optical properties, such as surface plasmon resonance, enabling accurate detection of biomolecules or environmental toxins. Additionally, in catalysis, controlling aggregation ensures a higher surface area for reactions, improving catalytic efficiency. By optimizing the stability of AgNPs during synthesis and storage, industries can refine production processes to create tailored nanoparticles for targeted uses in medicine, electronics, and water treatment systems.

Acknowledgments

Centre for Micro and Nanotechnology UR is acknowledged for HR SEM imaging.

References

[1] O. Pryshchepa, P. Pomastowski, B. Buszewski, „Silver nanoparticles: Synthesis, investigation techniques, and properties”, *Advances in Colloid and Interface Science*, t. 284, s. 102246, paź. 2020, doi: 10.1016/j.cis.2020.102246.

[2] P. Tan, H. Li, J. Wang, S. C. B. Gopinath, „Silver nanoparticle in biosensor and bioimaging: Clinical perspectives”, *Biotechnology and Applied Biochemistry*, t. 68, nr 6, s. 1236–1242, 2021, doi: 10.1002/bab.2045.

[3] L. Zhang, H. Jiang, W.-X. Wang, „Subcellular Imaging of Localization and Transformation of Silver Nanoparticles in the Oyster Larvae”, *Environ. Sci. Technol.*, t. 54, nr 18, s. 11434–11442, wrz. 2020, doi: 10.1021/acs.est.0c03342.

[4] A. Bouafia *et al.*, „The Recent Progress on Silver Nanoparticles: Synthesis and Electronic Applications”, *Nanomaterials*, t. 11, nr 9, Art. nr 9, wrz. 2021, doi: 10.3390/nano11092318.

[5] L. Xu, Y.-Y. Wang, J. Huang, C.-Y. Chen, Z.-X. Wang, H. Xie, „Silver nanoparticles: Synthesis, medical applications and biosafety”, *Theranostics*, t. 10, nr 20, s. 8996–9031, lip. 2020, doi: 10.7150/thno.45413.

[6] R. R. Miranda, I. Sampaio, V. Zucolotto, „Exploring silver nanoparticles for cancer therapy and diagnosis”, *Colloids and Surfaces B: Biointerfaces*, t. 210, s. 112254, luty 2022, doi: 10.1016/j.colsurfb.2021.112254.

[7] A. Kołodziej, A. Płaza-Altamer, J. Nizioł, T. Ruman, „Infrared pulsed fiber laser-produced silver-109-nanoparticles for laser desorption/ionization mass spectrometry of carboxylic acids”, *International Journal of Mass Spectrometry*, t. 474, s. 116816, kwi. 2022, doi: 10.1016/j.ijms.2022.116816.

[8] A. Płaza-Altamer, A. Kołodziej, Z. Krupa, J. Nizioł, T. Ruman, „Infrared pulsed fiber laser-produced gold and silver-109 nanoparticles for laser desorption/ionization mass spectrometry of steroid hormones”, *Rapid Communications in Mass Spectrometry*, t. 37, nr 20, s. e9621, 2023, doi: 10.1002/rcm.9621.

[9] J. Nizioł *et al.*, „Localization of Metabolites of Human Kidney Tissue with Infrared Laser-Based Selected Reaction Monitoring Mass Spectrometry Imaging and Silver-109 Nanoparticle-Based Surface Assisted Laser Desorption/Ionization Mass Spectrometry Imaging”, *Anal. Chem.*, t. 92, nr 6, s. 4251–4258, mar. 2020, doi: 10.1021/acs.analchem.9b04580.

[10] K. Ossoliński *et al.*, „Monoisotopic silver nanoparticles-based mass spectrometry imaging of human bladder cancer tissue: Biomarker discovery”, *Advances in Medical Sciences*, t. 68, nr 1, s. 38–45, mar. 2023, doi: 10.1016/j.advms.2022.12.002.

[11] A. L. González, C. Noguez, J. Beránek, A. S. Barnard, „Size, Shape, Stability, and Color of Plasmonic Silver Nanoparticles”, *J. Phys. Chem. C*, t. 118, nr 17, s. 9128–9136, maj 2014, doi: 10.1021/jp5018168.

[12] W. Luo, W. Hu, S. Xiao, „Size Effect on the Thermodynamic Properties of Silver Nanoparticles”, *J. Phys. Chem. C*, t. 112, nr 7, s. 2359–2369, luty 2008, doi: 10.1021/jp0770155.

[13] J. Helmlinger *et al.*, „Silver nanoparticles with different size and shape: equal cytotoxicity, but different antibacterial effects”, *RSC Advances*, t. 6, nr 22, s. 18490–18501, 2016, doi: 10.1039/C5RA27836H.

[14] X. Li J. J. Lenhart, „Aggregation and Dissolution of Silver Nanoparticles in Natural Surface Water”, *Environ. Sci. Technol.*, t. 46, nr 10, s. 5378–5386, maj 2012, doi: 10.1021/es204531y.

[15] A. Płaza, A. Kołodziej, J. Nizioł, T. Ruman, „Laser Ablation Synthesis in Solution and Nebulization of Silver-109 Nanoparticles for Mass Spectrometry and Mass Spectrometry Imaging”, *ACS Meas. Sci. Au*, t. 2, nr 1, s. 14–22, luty 2022, doi: 10.1021/acsmeasuresciau.1c00020.

[16] X. Li, J. J. Lenhart, H. W. Walker, „Dissolution-Accompanied Aggregation Kinetics of Silver Nanoparticles”, *Langmuir*, t. 26, nr 22, s. 16690–16698, lis. 2010, doi: 10.1021/la101768n.

[17] I. Römer, T. A. White, M. Baalousha, K. Chipman, M. R. Viant, J. R. Lead, „Aggregation and dispersion of silver nanoparticles in exposure media for aquatic toxicity tests”, *Journal of Chromatography A*, t. 1218, nr 27, s. 4226–4233, lip. 2011, doi: 10.1016/j.chroma.2011.03.034.

[18] T. C. Prathna, N. Chandrasekaran, A. Mukherjee, „Studies on aggregation behaviour of silver nanoparticles in aqueous matrices: Effect of surface functionalization and matrix composition”, *Colloids and Surfaces A: Physicochemical and Engineering Aspects*, t. 390, nr 1, s. 216–224, paź. 2011, doi: 10.1016/j.colsurfa.2011.09.047.

[19] O. A. Yeshchenko, I. M. Dmitruk, A. A. Alexeenko, A. V. Kotko, J. Verdal, i A. O. Pinchuk, „Size and Temperature Effects on the Surface Plasmon Resonance in Silver Nanoparticles”, *Plasmonics*, t. 7, nr 4, s. 685–694, grudz. 2012, doi: 10.1007/s11468-012-9359-z.